Journal of Glaciology

Estimating glacier ice thickness and yield strength using surface elevation and the perfect-plastic approximation

Tanner May and Jeremy Bassis

Climate and Space Sciences and Engineering Department, University of Michigan, Ann Arbor, MI, USA

Article

Cite this article: May T, Bassis J (2025) Estimating glacier ice thickness and yield strength using surface elevation and the perfect-plastic approximation. *Journal of Glaciology* **71**, e128, 1–13. https://doi.org/10.1017/jog.2025.10091

Received: 29 May 2025
Revised: 20 August 2025
Accepted: 17 September 2025

Keywords:
alpine glaciers; bed topography; ice thickness; inversion modeling; yield strength

Corresponding author: Tanner May; Email: tannerma@umich.edu

Abstract

Our ability to accurately quantify the total ice volume in glaciers and the loss of glacier volume, discharge and freshwater in response to climate change is limited by a paucity of ice thickness and bed topography observations. Consequently, glacial ice thickness is often inferred indirectly from more easily obtained surface measurements. Here, we present a simple inversion building on the assumption of perfect plasticity. In the traditional perfect-plastic approximation, the ice thickness (or bed) can be inferred from the surface elevation and yield strength. Here, we extend this to demonstrate that, provided glaciers are changing, we can simultaneously determine the yield strength and bed topography from observations of surface elevation alone. We demonstrate that the ice thicknesses and bed topographies we infer perform comparably to other inversions documented in the Ice Thickness Models Intercomparison eXperiment. Unlike other inversions, we do not require surface mass balance or glacier velocities, which can be inaccurate and difficult to obtain. Given the increasing availability of high-resolution surface elevation data, it may be possible to apply this method to glaciers worldwide to better constrain the ice thickness, bed topography and volume of glaciers globally.

1. Introduction

Climate change is forcing the retreat and diminishment of glaciers worldwide (Haeberli and Beniston, 1998; Dyurgerov and Meier, 2000; Hock and Huss, 2021; Rounce and others, 2023). The associated water runoff, driven by melting glaciers, presents considerable ecological and societal hazards, including flooding, habitat destruction, depletion of freshwater resources and sea-level rise (Meier, 1984; Alley and others, 2005; Zhang and others, 2017). Moreover, glaciers are currently the dominant contributors to current rates of non-steric sea level rise, outpacing the Antarctic and Greenland ice sheets (Zemp and others, 2019; Hugonnet and others, 2021). Projections of sea level rise contributions by alpine glaciers are constrained by total glacier volume and are thus sensitive to bed topography (Radić and Hock, 2011; Marzeion and others, 2012). Determining the volume and mass loss of glacier ice is crucial for projecting the precise timing and magnitude of future effects as glaciers continue to shrink worldwide (Jury and others, 2019; Rounce and others, 2023; Yang and others, 2023). However, current estimates of glacier volume are often poorly constrained due to a sparsity of input data (such as surface mass balance or velocity measurements) (Farinotti and others, 2019; Millan and others, 2022; Hock and others, 2023) or reliance on equally sparse in-situ ice thickness measurements required for model calibration. Existing methods often disagree on the ice thickness of glaciers worldwide, and this tension has increased with recent studies suggesting that prior methods may be overestimating glacier volume globally, particularly in regions such as High Mountain Asia, and the Greenland and Antarctic peripheries (Farinotti and others, 2019; Millan and others, 2022).

Estimating total glacial surface area or change in terminus position is relatively straightforward using airborne photography or satellite imagery (Paul and others, 2013). Glacier ice thickness, by contrast, is notoriously difficult to quantify, with only sparse direct observations of ice thickness available (Welty and others, 2020; Hock and others, 2023). As a result, determining glacial thickness (and volume) remains challenging for most glaciers, especially for glaciers in remote or data-poor regions. Instead, ice thickness is often inferred using surface characteristics of the glacier (Farinotti and others, 2017, 2021).

Many existing glacial thickness estimation methods ingest various measurable surface properties, such as surface mass balance (Farinotti and others, 2009; Huss and Farinotti, 2012; Clarke and others, 2013; Michel and others, 2013; Morlighem and others, 2017; Rabatel and others, 2018) and/or velocity (Gantayat and others, 2014; Rabatel and others, 2018; Sattar and others, 2019) into equations of mass conservation and use this information to invert for ice thickness (Morlighem and others, 2017). Many of these methods also require quantities such as ice temperature and basal friction (McNabb and others, 2012;

© The Author(s), 2025. Published by Cambridge University Press on behalf of International Glaciological Society. This is an Open Access article, distributed under the terms of the Creative Commons Attribution licence (http://creativecommons.org/licenses/by/4.0), which permits unrestricted re-use, distribution and reproduction, provided the original article is properly cited.

https://doi.org/10.1017/jog.2025.10091 Published online by Cambridge University Press

Farinotti and others, 2017; Woodard and others, 2021) that are difficult to measure and are often inferred as part of the inversion. This is especially true of mass balance, where snowfall in mountainous regions can have large variations between adjacent glaciers or even between branches of the same glacier.

An alternative and much simpler approach utilizes the perfect-plastic approximation to estimate glacier thicknesses and underlying bed topography. Recent studies have shown that ice at both hard and deformable beds obeys a nearly plastic sliding law except for when slip velocities are low (e.g. Minchew and Joughin, 2020; Zoet and Iverson, 2020; Helanow and others, 2021). Moreover, the perfect-plastic approximation has been previously applied to model glacier evolution (Ultee and Bassis, 2017; Bassis and Ultee, 2019) and has long been used to invert for glacier thickness (Nye, 1952; Linsbauer and others, 2009; Li and others, 2012; Frey and others, 2014; Chen and others, 2022). Although the perfect-plastic approximation does not require mass balance, velocity or temperature as inputs, previous iterations of the perfect-plastic approximation have required *a priori* specification of the glacier yield strength (Linsbauer and others, 2009; Clarke and others, 2013; Frey and others, 2014; Chen and others, 2022). Given that the yield strength may vary significantly between glaciers, this represents an obstacle to using the perfect-plastic approximation in large-scale glacier inversions. To overcome this barrier, we explore a method based on the perfect-plastic approximation that requires no *a priori* knowledge or parameterizations of the yield strength.

Here, we extend previous methods that use the perfect-plastic approximation and show that, provided the perfect-plastic approximation is valid and glaciers are changing, we only need two easily obtained quantities to determine the bed topography uniquely: two maps of surface elevation at different times or rates of surface elevation change and a reference elevation map. We demonstrate that these two quantities produce self-consistent bed topography and yield strength estimations without requiring the specification of additional quantities. The structure of this paper is as follows: first, we introduce a set of reference glaciers previously used by the Ice Thickness Models Intercomparison eXperiment (hereafter ITMIX) (Farinotti and others, 2017). Next, we review the perfect-plastic approximation and show how we exploit measurements of surface elevation change to infer both glacier ice thickness and yield strength simultaneously. Finally, applying our method to a set of reference glaciers, we demonstrate that our method produces comparable inversion results to others in the ITMIX experiments (Farinotti and others, 2017, 2021), and discuss how our method may offer the potential for regional and global-scale glacier analysis given the increasingly widespread availability of measurements of glacier surface elevation and thickness change (e.g. Hugonnet and others, 2021).

2. Studied glaciers

Following ITMIX (Farinotti and others, 2017), we test our inversion on several reference glaciers: the Svalbard ice cap Austfonna, the Scandinavian glacier Hellstugubreen, the Swiss glacier Unteraargletscher (hereafter Unteraar) and the many glaciers of Mount Elbrus in Russia. We choose this selection of glaciers because Farinotti and others (2017) provides the reference surface digital elevation models (DEMs) and change rates in ice thickness ($\frac{\partial h}{\partial t}$)(Fig. 1) that we require as inputs. We use these surface elevation and thickness change maps, together with point observations of the bed, also provided by ITMIX, to test the fidelity of our inversions. This geographically and dynamically diverse set of glaciers (Table 1) enables us to assess inversion performance by directly comparing results and error statistics with other inversion methods across the same reference glaciers.

3. Statistics

We employ Mean Absolute Error (MAE) and Mean Bias Error (MBE) to assess our inversion's performance against ice thickness measurements obtained from echo-radar ground truth bed elevation measurements obtained from ITMIX (Farinotti and others 2017, 2021), defined as,

$$\mathrm{MAE} = \frac{1}{M}\sum_{i=1}^{M} |b^i - B^i|, \tag{1}$$

$$\mathrm{MBE} = \frac{1}{M}\sum_{i=1}^{M} b^i - B^i, \tag{2}$$

where M is the total number of ground truth bed observations, b^i and B^i are estimated and observed ice thicknesses, respectively, and superscript i denotes individual points of known thickness. MAE quantifies the average variance of the estimated bed from bed depth observations. In contrast, MBE gauges the bias relative to bed elevation measurements, which is useful for quantifying whether the inversion overestimates or underestimates total ice volume.

Normalizing these error statistics by mean glacier thickness enables a more meaningful comparison of errors across glaciers, as it accounts for the relative significance of the errors relative to the size of the glaciers. We introduce the Coefficient of Variance (CV) counterparts by normalizing MAE and MBE by the mean measured glacier thickness $\bar{H}$ at the time nearest to when thickness observations were collected,

$$\mathrm{CV(MAE)} = \frac{1}{\bar{H}}\left(\mathrm{MAE}\right), \tag{3}$$

$$\mathrm{CV(MBE)} = \frac{1}{\bar{H}}\left(\mathrm{MBE}\right). \tag{4}$$

Next, we review the perfect-plastic approximation and demonstrate how it can be exploited to estimate glacier ice thickness and bed topography given only repeat elevation data that are becoming increasingly readily available by aerial and satellite imagery.

4. Theory, method, and results

4.1. Review of the perfect-plastic approximation

First described by Nye (1951), Nye's original treatment of the perfect-plastic approximation assumes that glacier ice can be treated as a rigid body beneath a material yield strength, τ_y. Once the shear stress at the bed exceeds the yield strength, the ice deforms rapidly to reduce the stress to the yield strength (e.g. Ultee and Bassis, 2016; Bassis and Ultee, 2019). However, because in the shallow-ice approximation, the shear stress increases with depth and reaches a maximum at the ice-bed interface, the perfect-plastic approximation is also appropriate when longitudinal stresses in the glacier are small and the sliding law at the ice-bed interface can be approximated as plastic (Ultee and Bassis, 2016, 2017; Bassis and Ultee, 2019; Zoet and Iverson, 2020). The perfect-plastic approximation provides a relationship between ice thickness $h(x, y, t)$, surface slope $\alpha(x, y, t)$ and yield strength τ_y (Nye, 1951; Paterson, 1970):

https://doi.org/10.1017/jog.2025.10091 Published online by Cambridge University Press

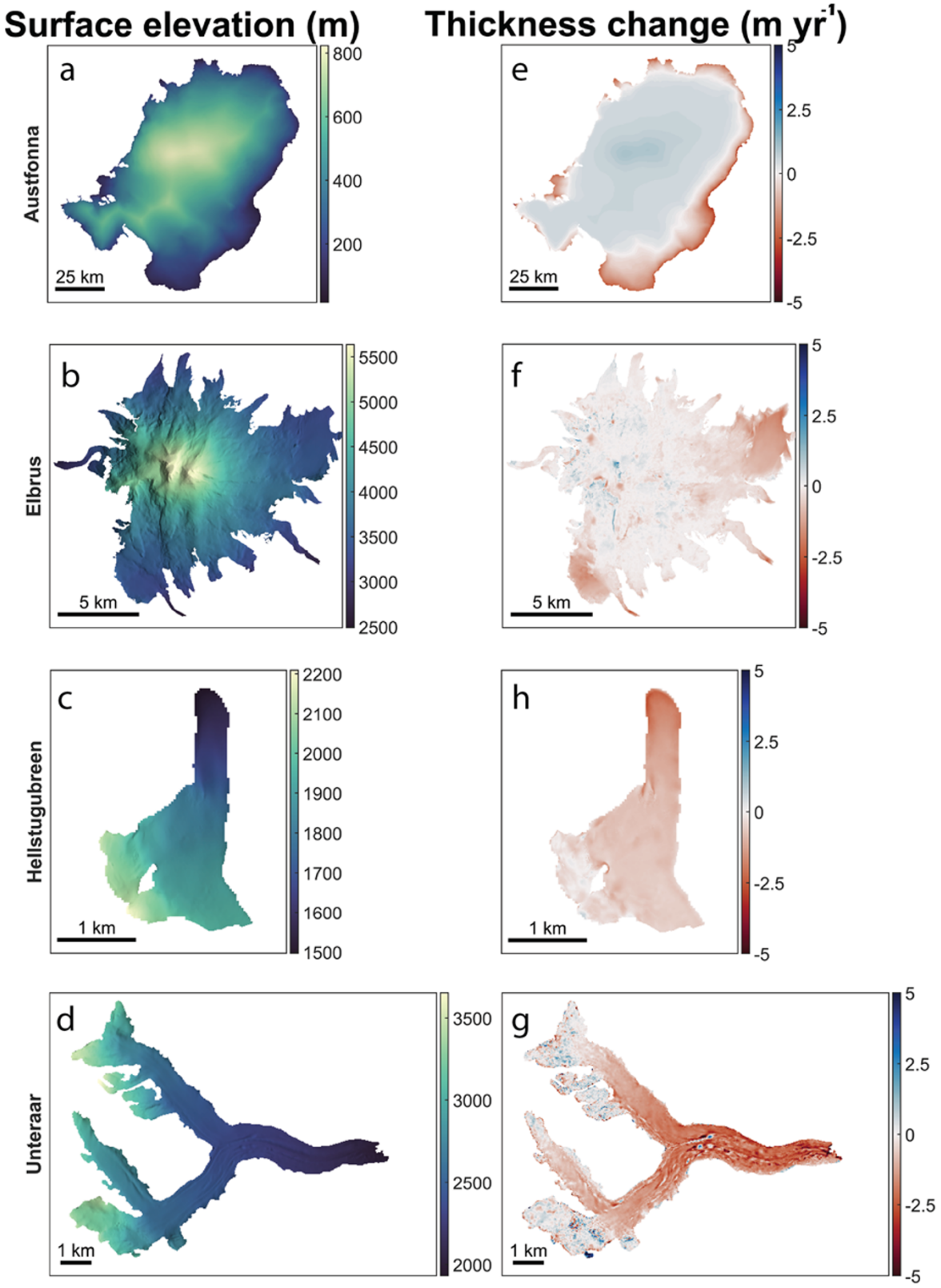


Figure 1. Subset of digital elevation models (left, panels a through d) and rates of thickness change (right, panels e through g) for each of the four reference glaciers we use to test our inversion in this study.

https://doi.org/10.1017/jog.2025.10091 Published online by Cambridge University Press

Table 1. Reference glaciers and quantities relevant to the presented inversion. All input data are sourced directly from the Ice Thickness Models Intercomparison eXperiment (ITMIX) (Farinotti and others, 2017).

Glacier Name	DEM year	$\frac{\partial h}{\partial t}$ years	Resolution (m)	Avg. thickness (m)	Bed measurements (M)
Austfonna	2007	2003-2009	300	353	5923
Elbrus	1997	1957-2007	30	58	4076
Hellstugubreen	2009	1997-2009	10	104	455
Unteraar	2003	1997-2003	25	232	1265

Table 2. Relevant parameters used in our inversion. The values of all quantities are considered variables except, $\rho = 910$ kg $\cdot$ m^{-3} and $g = 9.8$ m $\cdot$ s^{-2}.

Symbol	Quantity	Units
τ	Yield strength	Pa
ρ	Density of ice	kg $\cdot$ m^{-3}
g	Gravity	m $\cdot$ s^{-2}
h	Ice thickness	m
s	Surface Elevation	m a.s.l.
α	Surface slope	deg
b	Bed elevation	m a.s.l.

$$\tau_y = f \rho g h \sin \alpha, \tag{5}$$

where we have suppressed the dependence of variables on position (x, y) and time t for notational convenience. We define the surface slope, α, as a positive definite down-slope quantity between 0 and 90 degrees (Appendix A) using the method of finite differences (Figure A1) , ρ is the density of ice and g is the acceleration due to gravity (Table 2). The shape factor f incorporates the effect of lateral geometry (Nye, 1965; Paterson, 1970). This has been included in other perfect-plasticity-based inversions (Li and others, 2012; Van Wyk de Vries and others, 2022). The effect of the shape factor, f, however, introduces an additional parameter which, in our study, can ultimately be combined with the yield strength to result in an effective yield strength $\tau = \frac{\tau_y}{f}$ to write: (Nye, 1951; Paterson, 1970)

$$\tau = \rho g h \sin \alpha. \tag{6}$$

As first noted by Nye (1952), if we can measure the ice surface and assume a yield strength, we can rearrange Equation (6) to determine the ice thickness h:

$$h = \frac{\tau}{\rho g \sin \alpha}. \tag{7}$$

More usefully, defining the ice surface $s(x, y)$ and bottom $b(x, y)$ such that $h(x, y) = s(x, y) - b(x, y)$, the bed topography $b(x, y)$ can be deduced from Equation (7) solely from measurements of surface elevation (e.g. Linsbauer and others, 2009, 2012; Frey and others, 2014):

$$b(x, y) = s(x, y, t) - \frac{\tau}{\rho g \sin \alpha(x, y, t)}. \tag{8}$$

The challenge is that, although surface elevation (and slope) can increasingly be measured from airborne and spaceborne measurements, we have to make assumptions about the yield strength to apply Equation (8) to estimate the bed (e.g. Nye, 1952; Haeberli and Hoelzle, 1995; Linsbauer and others, 2012; Clarke and others, 2013; Frey and others, 2014; Chen and others, 2022; Van Wyk de Vries and others, 2022). This is problematic because the yield strength can vary between glaciers—or even spatially within a single glacier—in ways that heuristic parameterizations of the yield strength may not capture (Gowan and others, 2023).

4.2. Evolving glaciers and the perfect-plastic approximation

If both the bed elevation $b(x, y)$ and yield strength τ are time-independent, we can interpret Equation (8) as a single equation for both yield strength τ and bed topography $b(x, y)$: if we know one of these quantities, we can infer the other. However, for glaciers with measurements of rates of surface elevation or thickness change, we have additional information that we can use to determine both the bed topography and yield strength simultaneously.

In the following, we present a novel method for estimating bed topography and yield strength. The first step in our routine is to approximate the assumption of perfect plasticity as purely local and spatially variable, and to estimate the bed topography and yield strength for every point on the glacier surface where we have two independent elevation measurements. As we shall see, this approach can easily be contaminated by noise in elevation data, yielding spurious negative yield strengths and ice thicknesses. To rectify this, our method has two additional steps: first, we filter out outliers, then impose a spatially uniform yield strength for each glacier, thereby solving an over-determined system using standard least-squares to find a single yield strength for each glacier.

4.3. Step 1: Spatially variable yield strength with no regularization

If we have independent measurements of glacier surface elevations at times t_1 and t_2, we can recast Equation (8) in the form of two equations with two unknowns:

$$b(x, y) = s(x, y, t_1) - \frac{\tau(x, y)}{\rho g \sin \alpha(x, y, t_1)}, \tag{9}$$

$$b(x, y) = s(x, y, t_2) - \frac{\tau(x, y)}{\rho g \sin \alpha(x, y, t_2)}. \tag{10}$$

Equations (9) and (10) provide a system of equations for the unknown bed $b(x, y)$ *and* yield strength $\tau(x, y)$. This motivates our approach to using the perfect-plastic approximation for a simultaneous inversion of bed topography and yield strength. For glaciers that are evolving (and taking care to avoid regions of the glacier where the glacier surface is nearly flat and surface slope approaches zero), we can use two surface DEMs $s_1 \equiv s(x, y, t_1)$ and $s_2 \equiv s(x, y, t_2)$ and then solve Equations (9) and (10) to determine bed $b(x, y)$ and yield strength τ simultaneously, avoiding the need to specify the yield strength separately. For example, given two DEMs, we can write Equations (9) and (10) in matrix form:

$$\begin{bmatrix} 1 & \frac{1}{\rho g \sin \alpha_1^i} \\ 1 & \frac{1}{\rho g \sin \alpha_2^i} \end{bmatrix} \begin{bmatrix} b^i \\ \tau^i \end{bmatrix} = \begin{bmatrix} s_1^i \\ s_2^i \end{bmatrix}, \tag{11}$$

where the superscript i denotes co-registered grid points in a pair of DEMs, and subscripts denote the time intervals such that $\alpha_1 \equiv \alpha(x, y, t_1)$ and $\alpha_2 \equiv \alpha(x, y, t_2)$. Alternatively, defining the difference in glacier surface elevation between times t_1 and

https://doi.org/10.1017/jog.2025.10091 Published online by Cambridge University Press

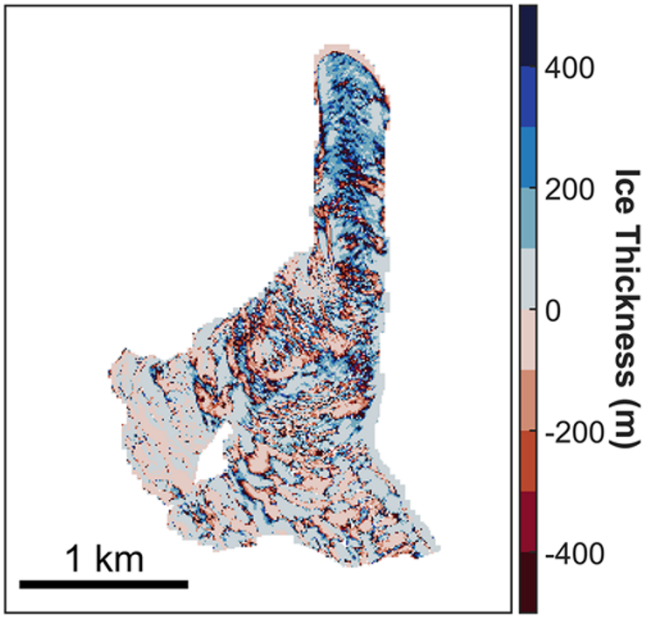


Figure 2. Negative yield strengths from Equation (12) contaminate ice thickness results with negative ice thicknesses for Hellstugubreen Glacier.

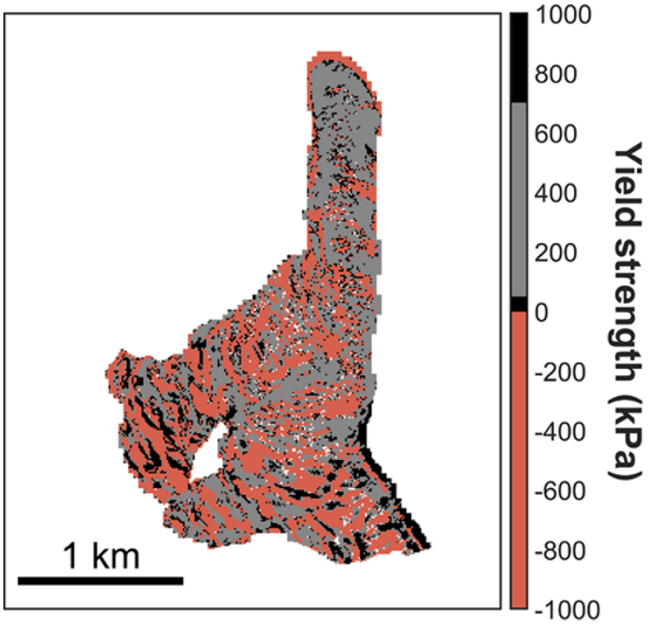


Figure 3. Yield strengths produced via Equation (12). We present grid points that produce negative yield strengths in red, and positive yield strength values falling outside the 15th and 85th percentiles in black. Here, only the grey grid points are ingested into Equation (14).

t_2, $\Delta s^i \equiv s_2^i - s_1^i$, and then subtracting Equation (9) from (10) and rearranging, we can find a single equation for the yield strength at every grid point:

$$\tau^i = \frac{\rho g \Delta s^i \sin\alpha_1^i \sin\alpha_2^i}{\sin\alpha_1^i - \sin\alpha_2^i}. \tag{12}$$

After solving for the yield strength using Equation (12), we can use Equation (9) or (10) to find the bed elevation at each grid point. Here, we estimate the surface slope α^i using central differences with a minimum slope regularization to prevent issues that arise in areas where the slope becomes small (Appendix A).

Figures 2 and 3 show thickness and yield strength results when applied to Hellstugubreen Glacier. The inversion produces nonphysical negative yield strengths in 39% of grid points in Hellstugubreen's interior. This failure implies issues with either some combination of the assumptions made or the data ingested. For instance, our method relies on the perfect-plastic approximation (a relatively crude approximation of ice dynamics) and the shallow-ice approximation, which limits application to large length scales compared to the ice thickness (e.g. Fowler and Larson, 1978). Similarly, noise in the input data may contaminate slope approximations and inversion results, suggesting a need to regularize the solution to obtain more sensible results. To avoid erroneous yield strengths and ice thicknesses, we filter grid points that produce spurious results in Equation (12) and assume the yield strength is approximately constant for each glacier, therefore constructing an overdetermined system to find a single, glacier-averaged yield strength. We discuss these additional steps in the following.

4.4. Step 2: Filter spurious results

To prevent noise in surface elevation measurements and slope estimates from skewing our inversion, we first use Equation (12) to identify regions resulting in negative yield strengths. We then filter out these areas and all other grid points that produce yield strength values outside the 15th and 85th percentiles from the remaining entries. We visualize this two-step filtering routine in Fig. 3.

4.5. Step 3: Spatially uniform yield strength

The first step in our method solves for the yield strength independently for every grid point. This makes the strong assumption that the perfect-plastic approximation applies locally at the scale of grid spacing of DEMs, and that the yield strength can also vary over this scale. In the second step, we filter out negative and outlier grid points to prevent spurious results. Next, we assume that the plastic approximation is only valid when averaged over a sufficiently large patch of the glacier bed and seek a glacier-averaged yield strength for simplicity.

We drop the superscript denoting grid points from τ and add an overline to denote a single, glacier-averaged value for yield strength, $\bar{\tau}$. We can then construct an objective function for the mean squared error (MSE) mismatch between modeled and observed surface elevation changes,

$$MSE = \frac{1}{N}\sum_{i=1}^{N}\left[\left(\frac{1}{\rho g \sin\alpha_2^i} - \frac{1}{\rho g \sin\alpha_1^i}\right)\bar{\tau} - \Delta s^i\right]^2, \tag{13}$$

where superscript i denotes individual grid-points, subscript denotes time, N is the total number of geographically co-registered points in a DEM pair. To find the best-fitting glacier-averaged yield strength $\bar{\tau}$, we minimize Equation (13) in a typical least-squares fashion (Björck, 1990). Remarkably, Equation (13) can be minimized analytically. The result is a single equation for our estimate of $\bar{\tau}$:

$$\bar{\tau} = \frac{\sum_{i=1}^{N}\left(\frac{\Delta s^i(\sin\alpha_1^i - \sin\alpha_2^i)}{\rho g \sin\alpha_1^i \sin\alpha_2^i}\right)}{\sum_{i=1}^{N}\left(\frac{\sin\alpha_1^i - \sin\alpha_2^i}{\rho g \sin\alpha_1^i \sin\alpha_2^i}\right)^2}. \tag{14}$$

We then use Equation (7), (9) or (10) to determine the ice thickness or bed topography from $\bar{\tau}$. Because our estimate of τ is now no longer exactly consistent with the assumption of perfect plasticity everywhere, the beds estimated at times t_1 and t_2 from

https://doi.org/10.1017/jog.2025.10091 Published online by Cambridge University Press

Equations (9) and (10) may differ slightly. In this study, we take the average of the two to create a single estimate for the glacier bed.

As a test, we first applied this approach to Hellstugubreen. Figure 3 shows the spatial distribution of negative and extreme yield strength values filtered out and not considered in Equation (14). Figure 4 panel h shows that when using only the filtered yield strengths, we estimate a physically plausible bed, whereas Equation (12) alone outputs negative yield strengths and ice thicknesses.

We next apply Equation (14) to four reference glaciers included in ITMIX: Austfonna, Elbrus, Hellstugubreen and Unteraar. Summary statistics for the reference glaciers are shown in Table 3. In Fig. 4, panels a through d display maps of inferred bed topography, and panels e through g show ice thickness for all the reference glaciers. Together, these illustrate how our inversion produces bed and thickness estimates without negative or spuriously large ice thicknesses in the inversion. The mean basal yield strength across all glaciers is ∼110 kPa, which is broadly consistent with previous results in the literature (Nye, 1951; Fischer, 2012; Li and others, 2012; Clarke and others, 2013; Zoet and Iverson, 2020; Van Wyk de Vries and others, 2022).

4.6. Validation with bed observations

Next, we validate ice thickness estimates against ice thickness measurements for each glacier from Farinotti and others (2017) to quantify the errors associated with our inversion. The number of thickness point measurements N used for validation, together with other relevant glacier data, is presented in Table 1.

Figure 5 shows observed versus estimated ice thicknesses for each of the four reference glaciers. Here, we observe that errors in our inferred ice thickness vary glacier by glacier. Although Hellstugubreen, our best-performing glacier, follows the zero-error line relatively well, our inversion tends to overestimate smaller ice thicknesses and underestimate large ice thicknesses for Austfonna. Elbrus, however, shows no clear trends but produces noisy results near the median ice thickness. We see from Fig. 5 and Table 3 that our inversion produces erroneously thin ice thickness estimations for Unteraar, with a large negative bias showing severe underestimation of ice thickness (-88% mean bias), and the yield strength would need to be much greater to match observations. This underestimation problem is not unique to our inversion method; other approaches in the ITMIX (Farinotti and others, 2017) suite struggle similarly to produce sufficiently thick ice thickness measurements for Unteraar in particular. Next, we compare our results to those of other methods in the ITMIX suite.

4.7. Comparison to existing ice thickness inversions

We compare our results to several ice thickness inversions to determine how well our simple inversion procedure compares to other inversions that participated in ITMIX (Farinotti and others, 2017). We see that—consistent with the statistics summarized in Table 3—our inversion performs comparably to other ice-thickness inversions, despite our method's simplicity. Our MAE and MBE fall within the IQR or outperform other inversions in three of the four glaciers studied, which we visualize in Fig. 6 using box-and-whisker plots. Figure 7 shows how our estimated bed compares to other inversions for a handful of glacier profiles. We demonstrate that our method produces bed geometry profiles comparable to other beds submitted to ITMIX.

5. Discussion

The perfect-plastic approximation-based inversion we introduce provides a simple method to estimate glacier thickness, bed topography and basal yield strength using solely surface elevation measurements. Despite our method's simplicity, we produce estimates of basal yield strength that agree with the current literature (O'Neel and others, 2005; Cuffey and Paterson, 2010; Li and others, 2012, Ultee and Bassis, 2016, 2017; Zoet and Iverson, 2020; Helanow and others, 2021), and bed topographies comparable to those obtained with more sophisticated inversion methods (Farinotti and others, 2017, 2021). We expect the perfect-plastic approximation to be most valid for glaciers on either hard or deformable beds where ice at the bed is sliding rapidly enough that sliding is approximately plastic (Zoet and Iverson, 2020; Helanow and others, 2021). By contrast, we anticipate that nearly static glaciers, which largely evolve due to surface mass balance with little ice dynamics, and surging glaciers, where the yield strength changes appreciably over the observational period, may challenge the perfect-plastic approximation. However, despite our test glaciers not neatly fitting into these categories, we find that our method performs as well as other methods for most glaciers tested, with near-zero mean-bias error when compared to bed observations for Austfonna, Elbrus and Hellstugubreen. This near-zero mean bias is likely a result of our choice to use a single yield strength for the entire glacier, which consequently means that we underestimate in some regions and overestimate in others, in ways that may cancel each other out in Equation (2). Nevertheless, this may be beneficial for regional-scale analyses, where the average accuracy over entire regions is preferred over minimizing errors for individual glaciers, as shown in other model description papers (e.g. Huss and Hock, 2015; Maussion and others, 2019). Our inversion does have some limitations, however, which we discuss in the following.

5.1. Inversion limitations

Our assumptions of a plastic rheology, unchanging bed topography, and static yield strength dictate particular relationships between observed changes in glacier surface elevation and slope, as explored in Equations (12) and (14). When these relationships are not satisfied, the inversion may fail to estimate yield strength and ice thickness accurately. This is the main drawback to Equation (12), where every point is treated independently. We suspect this is a consequence of noisy input data and/or applying the perfect-plastic approximation over length scales where the perfect-plastic approximation does not apply. Thus, applying the perfect-plastic approximation to a larger suite of test glaciers may better reveal conditions when the perfect-plastic approximation is likely to fail and provide erroneous results.

The steps explored in this paper, whether treating every point independently or considering all points of the glacier simultaneously, are only limiting cases in a spectrum of possible yield strength regularization routines. A potential drawback to our inversion is that a single glacier-averaged yield strength may not be sufficient to resolve the bed geometry of some particularly complex glaciers. We suspect that including a more generalized regularization that allows for spatially variable yield strength may yield more accurate estimates of ice thickness and bed topography for some glaciers. Still, we cannot discount the potential that our inversion method may perform poorly in some instances. A perfectly plastic rheology may not be suitable in some cases, particularly for

https://doi.org/10.1017/jog.2025.10091 Published online by Cambridge University Press

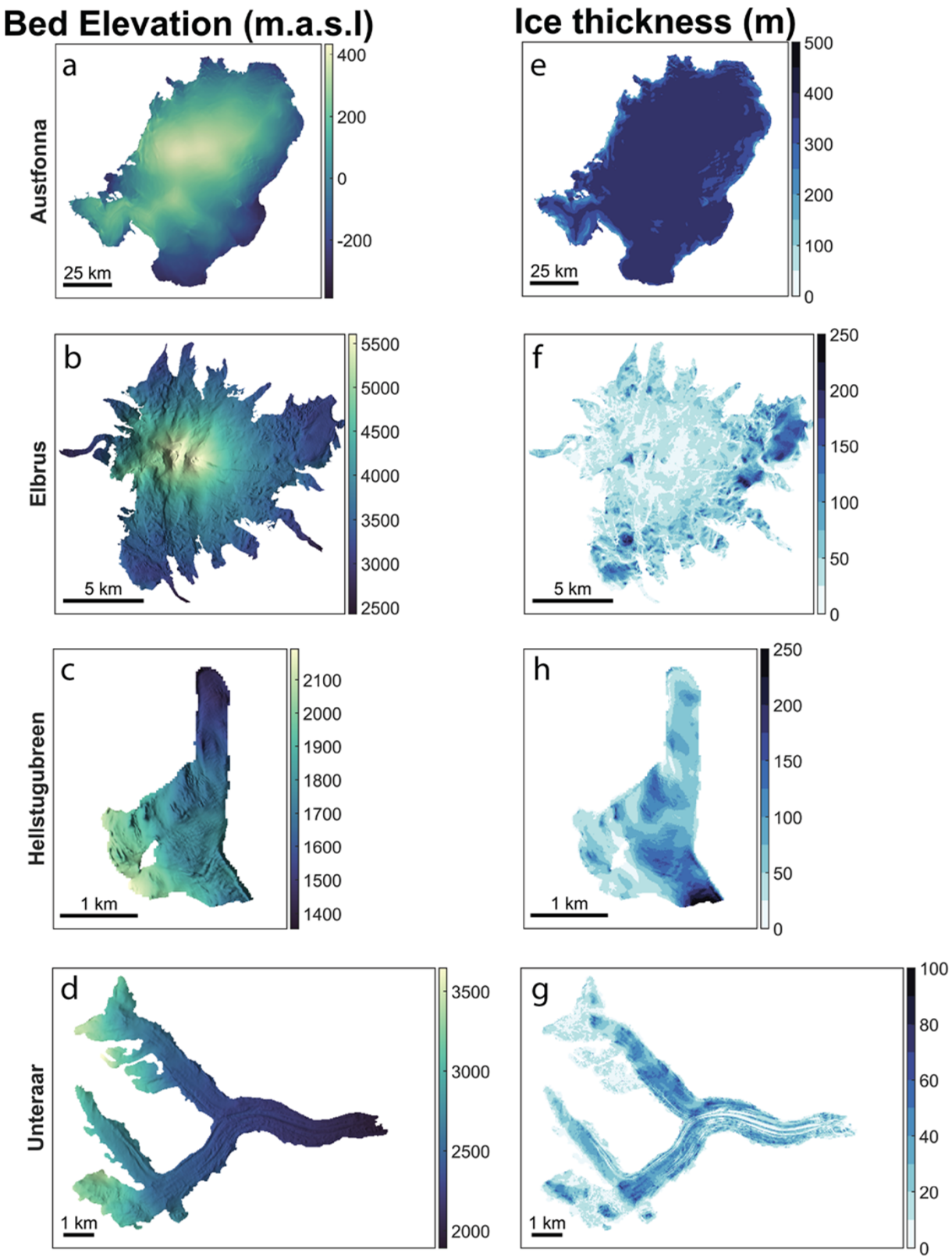


Figure 4. Bed topography (left, panels a through d) and ice thickness measurements (right, panels e through g) for the reference glaciers we use to test our inversion using Equation (14).

https://doi.org/10.1017/jog.2025.10091 Published online by Cambridge University Press

Table 3. Estimated yield strength, mean ice thickness, and error statistics for each of the four reference glaciers.

Glacier Name	$\bar{\tau}$ (kPa)	$\bar{h}$ (m)	MAE (m)	CV(MAE) (%)	MBE (m)	CV(MBE) (%)
Austfonna	183	361	85	24	8	2
Elbrus	107	57	29	50	0	0
Hellstugubreen	118	97	25	24	-7	-7
Unteraar	39	31	205	88	-204	-88

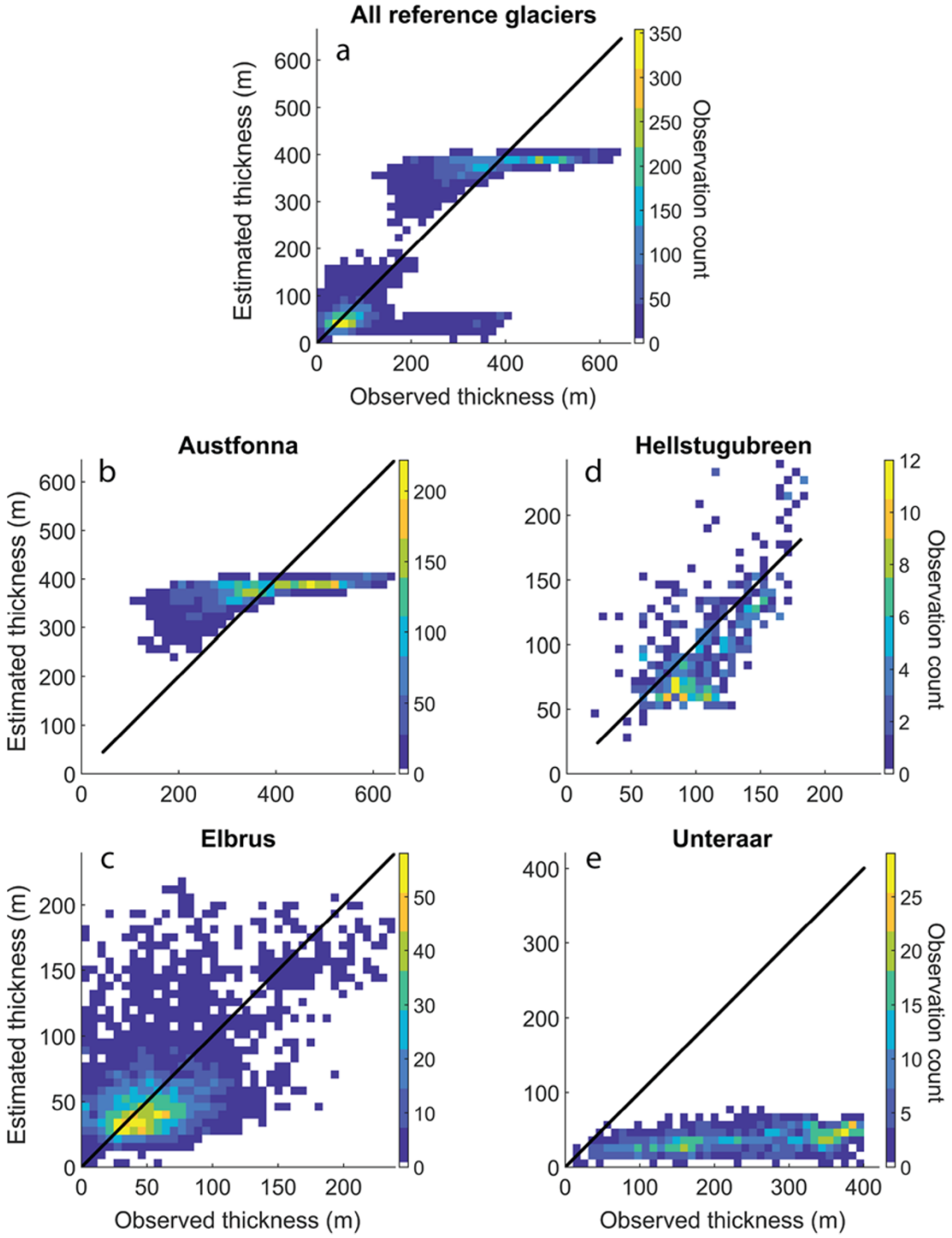


Figure 5. Error distribution heatmaps for each reference glacier studied, along with all points of known glacier bed depth.

https://doi.org/10.1017/jog.2025.10091 Published online by Cambridge University Press

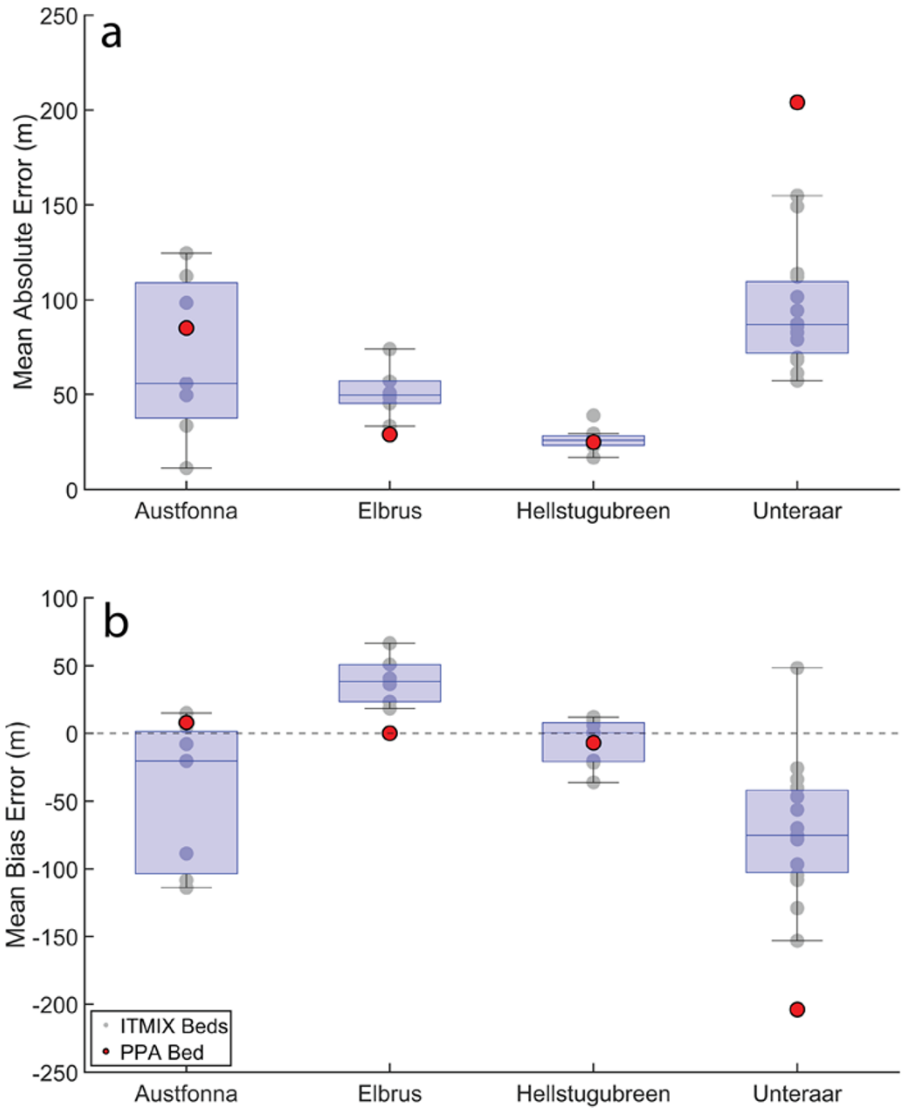


Figure 6. Box-and-whisker plots of errors for all inversion methods submitted to the Ice Thickness Models Intercomparison eXperiment (ITMIX) (Farinotti and others, 2017), together with our perfect-plastic approximation (PPA) bed errors for each of the reference glaciers considered. The blue box represents the IQR of model errors, and whiskers extend to the minimum and maximum non-outlier values. The number of ITMIX inversions per glacier are: Austfonna = 7, Elbrus = 6, Hellstugubreen = 8, Unteraar = 15 inversions.

glaciers that are surging. Additionally, it is possible that glaciers with changing beds (for example, Columbia Glacier, AK (Boldt Love and others, 2016)) may not satisfy the condition of time-independent bed geometry imposed in Equations (9), (10) and (11) in some areas, which may contribute to errors in bed topography for these glaciers. However, our inversion errors for the bed are often on the order of tens of meters; thus, even in regions with extreme sediment deposition rates, the assumption of a stagnant bed may not be entirely unjustified. Furthermore, given increased satellite coverage, it is possible that future inversions could improve upon ours by using multiple snapshots to infer a time-varying bed.

A major assumption of the perfect-plastic approximation is that subglacial topographical features manifest on the surface. Our inversion works in the reverse direction, with every surface characteristic being linked to subsurface geography. Therefore, estimates of bed topography and ice thickness can easily be contaminated by noise and errors in surface elevation measurements. To quantify the effect of surface elevation error on our results, we ran a suite of simple perturbation tests on our input data for the glacier Hellstugubreen.

5.2. Sensitivity tests

To better understand the effect of noisy input data, we perform a simple sensitivity analysis, shown in Table 4, by perturbing all of Hellstugubreen's input surface data grid cells (10-meter resolution) with uniformly distributed vertical noise. We introduce an error of between $\pm$ 1 meter to the reference surface elevation map and $\pm$ 0.1 meters per year to rates of thickness change. We find that heavy surface contamination can significantly decrease the estimated yield strength, resulting in thinner ice estimations that, on average, increase inversion error. We suspect noise in surface elevation measurements may be responsible for the spuriously thin ice thickness estimates for Unteraar, and that smoothing the surface maps before ingestion may improve our estimated glacier bed.

5.3. Data quality and surface smoothing

We find that smoothing the ITMIX surface elevation data before ingesting it into our inversion, or using different surface inputs entirely, recovers thicker ice thicknesses for Unteraar, thereby

https://doi.org/10.1017/jog.2025.10091 Published online by Cambridge University Press

reducing the error relative to observations. We smoothed ITMIX surface measurements at both times using a Gaussian-weighted filter with a standard deviation and filter radius comparable in size to Unteraar's mean observed ice thickness (about 230 m). Smoothing surface inputs in this manner results in a significantly improved bed for Unteraar, with error metrics MAE and MBE reducing to −103 meters (44%) and −84 meters (−36%), respectively. These improved metrics place our bed within the IQR of all Unteraar ITMIX inversions instead of being the worst-performing method. Of course, we do not necessarily know the ice thickness in advance for many glaciers, and hence, developing a more systematic regularization/smoothing approach may be necessary for estimating glacier ice thicknesses.

Upon ingesting alternative surface elevation measurements (ASTER GDEM 3.0) and thickness change products from Hugonnet and others (2021) into our inversion without smoothing, we again find that the MAE and MBE metrics for Unteraar drop significantly, with MAE decreasing to 81 meters (35%) and MBE to −33 meters (−14%). These analyses, combined with the reality that most methods from the ITMIX suite similarly struggle with Unteraar, suggest that our difficulties with Unteraar may not necessarily reflect sensitivity to characteristics specific to Unteraar, but to something inherent in the ITMIX data.

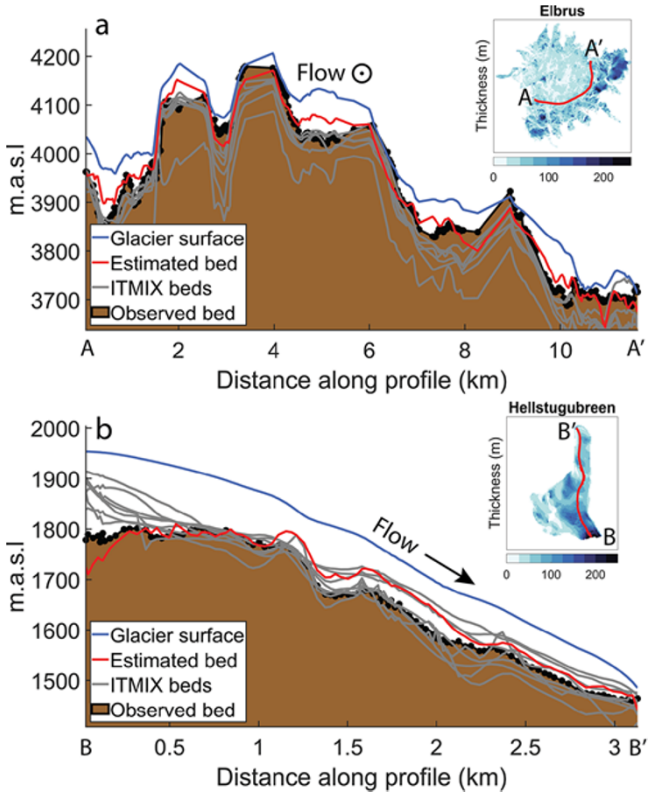


Figure 7. Panel a (10x vertical exaggeration): cross-sectional profile for Elbrus transverse to flow. Panel b (3x vertical exaggeration): cross-sectional profile for Hellstugubreen parallel to flow. A and B denote the transects' starting points, with A' and B' being endpoints, respectively. In both transects, the blue line is the ice surface, the brown area is the known bed reconstructed from point observations of the bed, the red is the estimated bed profile created by our inversion and the unlabeled grey lines are other ice thickness inversions submitted to ITMIX (Farinotti and others, 2017).

5.4. Suitability for global-scale glacier analysis

We believe our inversion method is well-suited for global studies of glacier ice thickness and potential sea level rise, owing to the relative abundance of readily available surface topography products that can be used as inversion inputs. There exist several DEMs providing worldwide surface elevation coverage (TanDEM-X, ASTER GDEM, NASADEM, SRTM, Copernicus DEM), regional DEMs (ArcticDEM, EuroDEM, USGS The National Map, among many others) and glacier thickness change products (Hugonnet and others, 2021), that together provide surface elevation measurements for practically all glaciers on Earth.

Moreover, our inversion can perform regional and global-scale computations covering entire regions in the Randolf Glacier Inventory at significantly less computational expense than many other inversion methods, needing only to solve Equation (14) once per glacier inverted. This computational affordability provides the flexibility to perform experiments that may be difficult for other global-scale inversions, such as sensitivity tests where we perturb inputs, interpolate data to different resolutions and even perform bootstraps to assess uncertainty.

6. Conclusions

We present a novel extension of the perfect-plastic approximation to infer glacier ice thickness, apply the approach to reference glaciers, and validate results against ice thickness observations. Our inversion method offers promising results for reconstructing subglacial bed topography and estimating glacier ice thickness. We demonstrate that with the perfect-plastic approximation, we create estimates of glacier ice thickness and bed elevation comparable to more sophisticated methods using minimal input data—only two measurements of glacier surface elevation separated in time. This makes our inversion particularly useful for poorly studied glaciers in remote areas and for glaciers that are changing. Given that the only data required are surface DEMs (which are becoming increasingly readily available) and georeferenced glacier outlines (available through the Randolph Glacier Inventory (Pfeffer and others, 2014)), we believe this method is suitable for large-scale global glacier analysis. We seek to expand upon this research by applying our inversion method globally to catalog ice thickness estimates for glaciers worldwide, combining knowledge of surface, slope, and yield strength features to infer subglacial conditions and their interactions in an ever-evolving cryosphere.

Table 4. Effects of adding uniform noise to surface inputs for Hellstugubreen Glacier on yield strength, Mean Absolute Error (MAE) and Mean Bias Error (MBE).

		Hellstugubreen		
Input	Perturbation	$\Delta\bar{\tau}$ (kPa)	Δ MAE (m)	Δ MBE (m)
Surface Elevation	$-1 \leq \delta s \leq 1$ (m)	-71	42	-61
Thickness change	$-.1 \leq \delta\frac{\partial h}{\partial t} \leq .1(\mathrm{m}\cdot\mathrm{yr}^{-1})$	-79	49	-68

https://doi.org/10.1017/jog.2025.10091 Published online by Cambridge University Press

Acknowledgements. I thank my advisor and co-author, Jeremy Bassis, along with everyone in the Vintage Glaciology Group, for their continued mentorship, support, and helpful discussions. I also thank the wonderful physics faculty at Centre College for encouraging me to pursue a doctoral program in the sciences. We thank Lizz Ultee and another unnamed reviewer for their insightful feedback during the preparation and review of this paper. This work is funded by DoE grant C3710, Framework for Antarctic System Science in E3SM, NASA grant 80NSSC22K0378 by the DOMINOS project, a component of the International Thwaites Glacier Collaboration (ITGC). Support from National Science Foundation (NSF: Grant 1738896) and Natural Environment Research Council (NERC: Grant NE/S006605/1).

References

Alley RB, Clark PU, Huybrechts P and Joughin I (2005) Ice-sheet and sea-level changes. *Science* **310**(5747), 456–460 doi: 10.1126/science.1114613

Bassis JN and Ultee L (2019) A thin film viscoplastic theory for calving glaciers: Toward a bound on the calving rate of glaciers. *Journal of Geophysical Research: Earth Surface* **124**(8), 2036–2055. doi: 10.1029/2019jf005160

Björck Å (1990) Least squares methods. *Handbook of Numerical Analysis*. Ciarlet PG & Lions JL Eds. Volume 1. Elsevier. 465-652. doi: 10.1016/S1570-8659(05)80036-5

Boldt Love K, Hallet B, Pratt TL and O'Neel S (2016) Observations and modeling of fjord sedimentation during the 30 year retreat of Columbia Glacier, AK. *Journal of Glaciology* **62**(234), 778–793. doi: 10.1017/jog.2016.67

Chen W and 6 others (2022) Towards ice-thickness inversion: an evaluation of global digital elevation models (DEMs) in the glacierized Tibetan plateau. *The Cryosphere* **16**(1), 197–218. doi: 10.5194/tc-16-197-2022

Clarke GKC and 6 others (2013) Ice volume and subglacial topography for western Canadian glaciers from mass balance fields, thinning rates, and a bed stress model. *Journal of Climate* **26**(12), 4282–4303 doi: 10.1175/jcli-d-12-00513.1

Cuffey KM and Paterson WSB (2010) *The physics of glaciers.*, 4th Edn. San Diego, CA: Academic Press

Dyurgerov MB and Meier MF (2000) Twentieth century climate change: Evidence from small glaciers. *Proceedings of the National Academy of Sciences* **97**(4), 1406–1411. doi: 10.1073/pnas.97.4.1406

Farinotti D, Huss M, Bauder A, Funk M and Truffer M (2009) A method to estimate the ice volume and ice-thickness distribution of alpine glaciers. *Journal of Glaciology* **55**(191), 422–430 doi: 10.3189/002214309788816759

Farinotti D and 39 others (2017) How accurate are estimates of glacier ice thickness? Results from ITMIX, the Ice Thickness Models Intercomparison eXperiment. *The Cryosphere* **11**(2), 949–970 doi: 10.5194/tc-11-949-2017

Farinotti D and 6 others (2019) A consensus estimate for the ice thickness distribution of all glaciers on earth. *Nature Geoscience* **12**(3), 168–173 doi: 10.1038/s41561-019-0300-3

Farinotti D and 19 others (2021) Results from the Ice Thickness Models Intercomparison eXperiment Phase 2 (ITMIX2). *Frontiers in Earth Science* **8** doi: 10.3389/feart.2020.571923

Fischer M (2012) *Application of a refined perfect-plasticity approach for empirical GIS-based basal shear stress modelling to now ice-free LIA glacier forefields in the Swiss Alps*. MSc Thesis, University of Zurich, Switzerland. doi: 10.13140/RG.2.1.2459.1123

Fowler AC and Larson DA (1978) On the flow of polythermal glaciers - I. Model and preliminary analysis. *Proceedings of the Royal Society of London. A. Mathematical and Physical Sciences* **363**(1713), 217–242. doi: 10.1098/rspa.1978.0165

Frey H and 9 others (2014) Estimating the volume of glaciers in the himalayan–karakoram region using different methods. *The Cryosphere* **8**(6), 2313–2333 doi: 10.5194/tc-8-2313-2014

Gantayat P, Kulkarni AV and Srinivasan J (2014) Estimation of ice thickness using surface velocities and slope: case study at Gangotri Glacier, India. *Journal of Glaciology* **60**(220), 277–282 doi: 10.3189/2014jog13j078

Gowan EJ, Hinck S, Niu L, Clason C and Lohmann G (2023) The impact of spatially varying ice sheet basal conditions on sliding at glacial time scales. *Journal of Glaciology* **69**(276), 1056–1070. doi: 10.1017/jog.2022.125

Haeberli W and Beniston M (1998) Climate change and its impacts on glaciers and permafrost in the Alps. *Ambio* **27**(4), 258–265.

Haeberli W and Hoelzle M (1995) Application of inventory data for estimating characteristics of and regional climate-change effects on mountain glaciers: a pilot study with the European Alps. *Annals of Glaciology* **21**, 206–212 doi: 10.3189/s0260305500015834

Helanow C, Iverson NR, Woodard JB and Zoet LK (2021) A slip law for hard-bedded glaciers derived from observed bed topography. *Science Advances* **7**(20). doi: 10.1126/sciadv.abe7798

Hock R and Huss M (2021) *Glaciers and climate change*, 157–176. Elsevier, ISBN 9780128215753 doi: 10.1016/b978-0-12-821575-3.00009-8

Hock R, Maussion F, Marzeion B and Nowicki S (2023) What is the global glacier ice volume outside the ice sheets? *Journal of Glaciology* **69**(273), 204–210. doi: 10.1017/jog.2023.1

Hugonnet R and 10 others (2021) Accelerated global glacier mass loss in the early twenty-first century. *Nature* **592**(7856), 726–731. doi: 10.1038/s41586-021-03436-z

Huss M and Farinotti D (2012) Distributed ice thickness and volume of all glaciers around the globe. *Journal of Geophysical Research: Earth Surface* **117**(F4), n/a–n/a doi: 10.1029/2012jf002523

Huss M and Hock R (2015) A new model for global glacier change and sea-level rise. *Frontiers in Earth Science* **3**. doi: 10.3389/feart.2015.00054

Jury MW and 6 others (2019) Climate projections for glacier change modelling over the himalayas. *International Journal of Climatology* **40**(3), 1738–1754. doi: 10.1002/joc.6298

Li H, Ng F, Li Z, Qin D and Cheng G (2012) An extended perfect-plasticity method for estimating ice thickness along the flow line of mountain glaciers: [1]. *Journal of Geophysical Research.Earth Surface* **117**(1).

Linsbauer A, Paul F and Haeberli W (2012) Modeling glacier thickness distribution and bed topography over entire mountain ranges with GlabTop: Application of a fast and robust approach. *Journal of Geophysical Research: Earth Surface* **117**, F03007. doi: 10.1029/2011jf002313

Linsbauer P, Hoelzle F, Frey M and Haeberli W (2009) The Swiss Alps without glaciers – a GIS-based modelling approach for reconstruction of glacier beds. In *Proceedings of Geomorphometry*. Zurich, Switzerland, pp. 243–247. doi: 10.5167/UZH-27834

Marzeion B, Jarosch AH and Hofer M (2012) Past and future sea-level change from the surface mass balance of glaciers. *The Cryosphere* **6**, 1295–1322. doi: 10.5194/tc-6-1295-2012

Maussion F and 14 others (2019) The Open Global Glacier Model (OGGM) v1.1. *Geoscientific Model Development* **12**, 909–931. doi: 10.5194/gmd-12-909-2019

McNabb R and 11 others (2012) Using surface velocities to calculate ice thickness and bed topography: a case study at Columbia Glacier, Alaska, USA. *Journal of Glaciology* **58**(212), 1151–1164. doi: 10.3189/2012jog11j249

Meier MF (1984) Contribution of small glaciers to global sea level. *Science* **226**, 1418–1421. doi: 10.1126/science.226.4681.1418

Michel L, Picasso M, Farinotti D, Bauder A, Funk M and Blatter H (2013) Estimating the ice thickness of mountain glaciers with an inverse approach using surface topography and mass-balance. *Inverse Problems* **29**, 035002. doi: 10.1088/0266-5611/29/3/035002

Millan R, Mouginot J, Rabatel A and Morlighem M (2022) Ice velocity and thickness of the world's glaciers. *Nature Geoscience* **15**, 124–129. doi: 10.1038/s41561-021-00885-z

Minchew B and Joughin I (2020) Toward a universal glacier slip law. *Science* **368**, 29–30. doi: 10.1126/science.abb3566

Morlighem M and 31 others (2017) BedMachine v3: Complete bed topography and ocean bathymetry mapping of Greenland from multibeam echo sounding combined with mass conservation. *Geophysical Research Letters* **44**, 11051-11061. doi: 10.1002/2017gl074954

Nye J (1951) The flow of glaciers and ice-sheets as a problem in plasticity. *Proceedings of The Royal Society A: Mathematical, Physical and Engineering Sciences*. **207**(1091), 554–572 doi: 10.1098/rspa.1951.0140

Nye JF (1952) A method of calculating the thicknesses of the ice-sheets. *Nature* **169**, 529–530. doi: 10.1038/169529a0

Nye JF (1965) The flow of a glacier in a channel of rectangular, elliptic or parabolic cross-section. *Journal of Glaciology* **5** (41), 661–690. doi: 10.3189/s0022143000018670

O'Neel S, Pfeffer WT, Krimmel R and Meier M (2005) Evolving force balance at Columbia Glacier, Alaska, during its rapid retreat. *Journal of Geophysical Research: Earth Surface* **110**(F3), F03012. doi: 10.1029/2005jf000292

Paterson WSB (1970) The sliding velocity of Athabasca Glacier, Canada. *Journal of Glaciology* **9**(55), 55–63. doi: 10.3189/s0022143000026794

Paul F and 20 others (2013) On the accuracy of glacier outlines derived from remote-sensing data. *Annals of Glaciology* **54**(63), 171–182 doi: 10.3189/2013AoG63A296

Pfeffer WT and 18 others (2014) The Randolph Glacier Inventory: a globally complete inventory of glaciers. *Journal of Glaciology* **60**(221), 537–552. doi: 10.3189/2014jog13j176

Rabatel A, Sanchez O, Vincent C and Six D (2018) Estimation of glacier thickness from surface mass balance and ice flow velocities: A case study on Argentière Glacier, France. *Frontiers in Earth Science* **6**, 112. doi: 10.3389/feart.2018.00112

Radić V and Hock R (2011) Regionally differentiated contribution of mountain glaciers and ice caps to future sea-level rise. *Nature Geoscience* **4**, 91–94. doi: 10.1038/ngeo1052

Rounce DR and 12 others (2023) Global glacier change in the 21st century: Every increase in temperature matters. *Science* **379**, 78–83. doi: 10.1126/science.abo1324

Sattar A, Goswami A, Kulkarni AV and Das P (2019) Glacier-surface velocity derived ice volume and retreat assessment in the Dhauliganga basin, central Himalaya – a remote sensing and modeling based approach. *Frontiers in Earth Science* **7**, 105. doi: 10.3389/feart.2019.00105

Ultee L and Bassis J (2016) The future is Nye: an extension of the perfect plastic approximation to tidewater glaciers. *Journal of Glaciology* **62**(236), 1143–1152. doi: 10.1017/jog.2016.108

Ultee L and Bassis JN (2017) A plastic network approach to model calving glacier advance and retreat. *Frontiers in Earth Science* **5**, 24. doi: 10.3389/feart.2017.00024

Van Wyk de Vries M, Carchipulla-Morales D, Wickert AD and Minaya VG (2022) Glacier thickness and ice volume of the Northern Andes. *Scientific Data* **9**(1) doi: 10.1038/s41597-022-01446-8

Welty E and 11 others (2020) Worldwide version-controlled database of glacier thickness observations. *Earth System Science Data* **12**, 3039–3055. doi: 10.5194/essd-12-3039-2020

Woodard JB, Zoet LK, Iverson NR and Helanow C (2021) Variations in hard-bedded topography beneath glaciers. *Journal of Geophysical Research: Earth Surface* **126**(9), e2021JF006326. doi: 10.1029/2021jf006326

Yang L and 6 others (2023) Historical and projected evolutions of glaciers in response to climate change in High Mountain Asia. *Environmental Research* **237**, 117037. doi: 10.1016/j.envres.2023.117037

Zemp M and 14 others (2019) Global glacier mass changes and their contributions to sea-level rise from 1961 to 2016. *Nature* **568**, 382–386. doi: 10.1038/s41586-019-1071-0

Zhang Q, Zhang F, Kang S and Cong Z (2017) Melting glaciers: Hidden hazards. *Science* **356**, 495–495. doi: 10.1126/science.aan4118

Zoet LK and Iverson NR (2020) A slip law for glaciers on deformable beds. *Science* **368**, 76–78. doi: 10.1126/science.aaz1183

Appendix A. Appendix - Numerics

This section contains technical details that underlie our model development.

A.1. Surface slope and regularization

For any given surface $s(x, y, t)$, we find the surface slope angle $\alpha(x, y, t)$ via approximation at each discrete point on the ice surface using central finite differences,

$$\frac{\partial s(x,y,t)}{\partial x} \approx \frac{s(x+\Delta x, y, t) - s(x-\Delta x, y, t)}{2\Delta x},$$
$$\frac{\partial s(x,y,t)}{\partial y} \approx \frac{s(x, y+\Delta y, t) - s(x, y-\Delta y, t)}{2\Delta y}, \tag{A1}$$

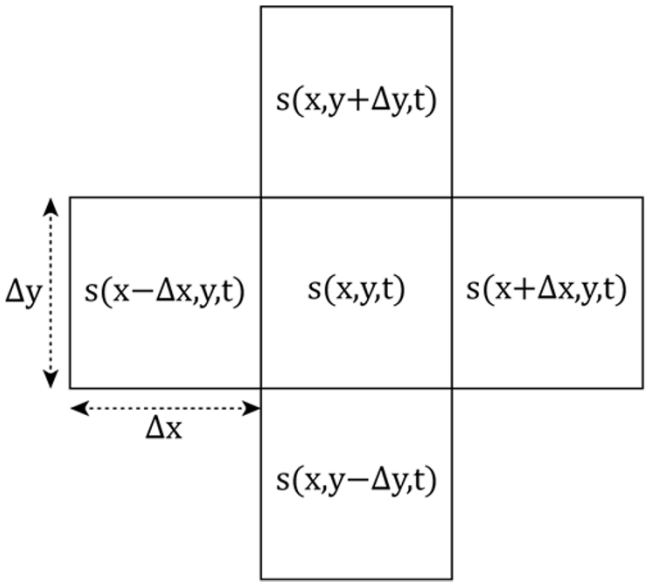


Figure A1. The setup for approximating surface slope using central finite differences described in Equation (A1) is visualized.

where we define x as the east-west direction, y as the north-south direction and Δx and Δy are grid cell spatial resolutions in the x and y directions in a Cartesian coordinate system, respectively.

Near the glacier edges, where central difference gradient estimation is not possible, a simpler forward or backward difference is taken, depending on which is necessary. Equation (A1) can be written as a vector,

$$\nabla \boldsymbol{s} = \begin{bmatrix} \frac{\partial s^i}{\partial x} \\ \frac{\partial s^i}{\partial y} \end{bmatrix}. \tag{A2}$$

Taking the arctangent of the magnitude of the gradient vector in Equation (A2) finds the slope angle θ that the surface makes relative to the horizontal.

$$\theta^i = \arctan ||\nabla \boldsymbol{s}|| = \arctan \sqrt{\left(\frac{\partial s^i}{\partial x}\right)^2 + \left(\frac{\partial s^i}{\partial y}\right)^2}. \tag{A3}$$

Following other studies (e.g. Farinotti and others, 2009, Li and others, 2012), we regularize all surface slope values by imposing a minimum slope limit (which we define as $\theta_0 = 3$ degrees) to avoid spuriously large ice thicknesses caused by nearly flat surface slopes. We define regularized slope values as,

$$\alpha^i = \sqrt{(\theta^i)^2 + (\theta_0)^2}, \tag{A4}$$

This method of regularization ensures that only small slopes are adjusted significantly. If $\theta^2 >> {\theta_0}^2$ then $\alpha^i \approx \theta^i$ and this regularization routine has little effect. In the methods section of this paper, all slope α values used and presented are regularized using this routine. Although our slope limiting constant could theoretically be tuned on a glacier-by-glacier basis, we define a single slope lower limit for simplicity. While individual glaciers may be sensitive to the choice of the lower limit of the slope, we find that it is not a significant factor when considering numerous glaciers in aggregate.

A.2. Surface input

We used all surface input data sourced from the ITMIX intercomparison project (Farinotti and others, 2017), which provides a DEM and gridded thickness change rates for each of the reference glaciers we present. A second surface elevation map can easily be produced by adding thickness change rates to a

https://doi.org/10.1017/jog.2025.10091 Published online by Cambridge University Press

preexisting map of surface elevations,

$$s_2^i = s_1^i + \frac{\partial h^i}{\partial t}\Delta t, \tag{A5}$$

where s_2 is surface elevation, $\frac{\partial h^i}{\partial t}$ is the rate of thickness change measured over the elapsed time $\Delta t = t_2 - t_1$. Assuming a non-changing bed, the thickness change is equal to the surface elevation change,

$$\frac{\partial h^i}{\partial t} = \frac{\partial s^i}{\partial t}, \tag{A6}$$

which is necessary to compute Equation (A5). Provided the time t_1 for surface elevation map s_1 is contained within the range which $\frac{\partial h^i}{\partial t}$ is valid, the choice of elapsed time Δt used in Equation (A5) is arbitrary and makes no significant impact on inversion results so long as Δt is valid within the provided surface measurement range.

https://doi.org/10.1017/jog.2025.10091 Published online by Cambridge University Press